remote sensing

MDPI

Article

UAV-LiDAR and RGB Imagery Reveal Large Intraspecific Variation in Tree-Level Morphometric Traits across Different Pine Species Evaluated in Common Gardens

Erica Lombardi [1,2,*], Francisco Rodríguez-Puerta [3], Filippo Santini [1,2], Maria Regina Chambel [4], José Climent [4], Víctor Resco de Dios [1,2] and Jordi Voltas [1,2]

[1] Joint Research Unit CTFC–AGROTECNIO–CERCA, University of Lleida, Av. Alcalde Rovira Roure 191, E-25198 Lleida, Spain
[2] Department of Crop and Forest Sciences, University of Lleida, Av. Alcalde Rovira Roure 191, E-25198 Lleida, Spain
[3] EiFAB-iuFOR, Campus Deques de Soria s/n, Universidad de Valladolid, E-42004 Soria, Spain
[4] Centro de Investigación Forestal (CIFOR-INIA/CSIC), Ctra. de La Coruña km 7.5, E-28040 Madrid, Spain
* Correspondence: erica.lombardi@udl.cat; Tel.: +34-973702226

Abstract: Remote sensing is increasingly used in forest inventories. However, its application to assess genetic variation in forest trees is still rare, particularly in conifers. Here we evaluate the potential of LiDAR and RGB imagery obtained through unmanned aerial vehicles (UAVs) as high-throughput phenotyping tools for the characterization of tree growth and crown structure in two representative Mediterranean pine species. To this end, we investigated the suitability of these tools to evaluate intraspecific differentiation in a wide array of morphometric traits for *Pinus nigra* (European black pine) and *Pinus halepensis* (Aleppo pine). Morphometric traits related to crown architecture and volume, primary growth, and biomass were retrieved at the tree level in two genetic trials located in Central Spain and compared with ground-truth data. Both UAV-based methods were then tested for their accuracy to detect genotypic differentiation among black pine and Aleppo pine populations and their subspecies (black pine) or ecotypes (Aleppo pine). The possible relation between intraspecific variation of morphometric traits and life-history strategies of populations was also tested by correlating traits to climate factors at origin of populations. Finally, we investigated which traits distinguished better among black pine subspecies or Aleppo pine ecotypes. Overall, the results demonstrate the usefulness of UAV-based LiDAR and RGB records to disclose tree architectural intraspecific differences in pine species potentially related to adaptive divergence among populations. In particular, three LiDAR-derived traits related to crown volume, crown architecture, and main trunk—or, alternatively, the latter (RGB-derived) two traits—discriminated the most among black pine subspecies. In turn, Aleppo pine ecotypes were partly distinguishable by using two LiDAR-derived traits related to crown architecture and crown volume, or three RGB-derived traits related to tree biomass and main trunk. Remote-sensing-derived-traits related to main trunk, tree biomass, crown architecture, and crown volume were associated with environmental characteristics at the origin of populations of black pine and Aleppo pine, thus hinting at divergent environmental stress-induced local adaptation to drought, wildfire, and snowfall in both species.

Keywords: Aleppo pine; black pine; crown architecture; climate adaptation; intraspecific variability; LiDAR; remote sensing; RGB

check for updates

Citation: Lombardi, E.; Rodríguez-Puerta, F.; Santini, F.; Chambel, M.R.; Climent, J.; Resco de Dios, V.; Voltas, J. UAV-LiDAR and RGB Imagery Reveal Large Intraspecific Variation in Tree-Level Morphometric Traits across Different Pine Species Evaluated in Common Gardens. *Remote Sens.* **2022**, *14*, 5904. https://doi.org/10.3390/rs14225904

Academic Editors: Andrea Hevia and Sandra Buján

Received: 13 October 2022
Accepted: 18 November 2022
Published: 21 November 2022

Publisher's Note: MDPI stays neutral with regard to jurisdictional claims in published maps and institutional affiliations.

Copyright: © 2022 by the authors. Licensee MDPI, Basel, Switzerland. This article is an open access article distributed under the terms and conditions of the Creative Commons Attribution (CC BY) license (https://creativecommons.org/licenses/by/4.0/).

1. Introduction

Progress in characterizing intraspecific differentiation in morphophysiological traits of forest trees can substantially increase our knowledge on their adaptability to environmental changes. Aboveground features such as total height, crown volume, and crown structure are strongly influenced by environmental factors such as temperature, light availability,

precipitation, or wind [1,2], as well as by disturbances such as fire or insect outbreaks [3–5]. They are also under genetic control and therefore subject to genotype by environment interactions [6]. Genetic changes and their associated interactions with the environment ultimately produce different phenotypes among individuals of the same species, and forest genetic trials are of paramount interest for understanding such phenotypic variation.

A major limitation when phenotyping forest trees in their adult stage in the context of evolutionary studies or breeding programs is the inherent complexity and time-consuming process of field-based measurements [7–9]. In this regard, high-throughput-phenotyping techniques have been developed in the last decade from different remote sensing tools [9,10]. In particular, light detection and ranging (LiDAR) and red–green–blue (RGB) imagery are effective tools with enough resolution for routine forestry applications [11,12].

RGB cameras are often mounted on unmanned aerial vehicles (UAVs), thereby providing aerial images of the visible spectrum (400–700 nm). By overlapping RGB images, it is possible to indirectly derive a point cloud holding 3D information. Airborne LiDAR scanning systems can be mounted on different platforms, including aircrafts or UAVs. LiDAR provides accurate 3D information about forest canopy cover since laser pulses can penetrate through vegetation. LiDAR is often considered to be a more effective approach than RGB imagery for the acquisition of stand and individual tree traits because it provides detailed information not only on the top of the tree crown, but also about the underlying branches and ancillary crown architecture [9,13]. However, RGB cameras can be mounted in smaller UAVs and are cheaper than LiDAR, thus making them a more practical and convenient tool in some circumstances. LiDAR and RGB imagery are already replacing traditional field-based measurements in certain forest operations, such as forest inventories [7,14], but the application of these technologies for the purpose of assessing phenotypic variation in genetic trials of forest species has been only seldom reported in the literature [10,15,16].

In this study, we investigated the accuracy of these remote sensing approaches (LiDAR- and RGB-based) mounted on UAVs to estimate commonly measured phenotypic traits such as tree height and biomass, but also other more complex traits related to crown architecture and volume. Particularly, we sought to evaluate if both remote sensing tools are valid to assess intraspecific differentiation in phenotypic traits of pine species. Previous attempts to assess the usefulness of these UAV-borne approaches have been restricted to hardwoods such as Eucalyptus spp. [10] or conifers such as *Picea abies* [15] or *Pseudotsuga menziesii* [17]. However, studies simultaneously evaluating both methods for their accuracy as phenotyping tools of forest genetic trials are still scarce [9], and they are non-existent in regard to pines.

In this context, we hypothesized that traits related to aboveground growth, such as the total height, trunk diameter (derived from allometric equations which consider crown area and total height), and tree biomass of adult pines, can be estimated with similar accuracy by using UAV-based remote sensing systems (LiDAR- and RGB-based) compared to traditional field methods, but more promptly. We also hypothesized that UAV–LiDAR and (to a lesser degree) UAV–RGB can provide reliable information of complex traits related to canopy architecture and canopy volume, whose estimation with traditional-field methods is time-consuming and ineffective [18]. To test these hypotheses, we the obtained remote sensing data of two Mediterranean pine species, *Pinus nigra* Arn. (European black pine) and *Pinus halepensis* Mill. (Aleppo pine), from two provenance genetic trials (or common gardens) located in Central–Western Spain. By using provenance trials, we aimed to describe intraspecific genetic variation in morphological traits derived from traditional field-based and high-throughput methods. In a common garden, trees of the same species, but belonging to populations having different geographic origins, grow under similar environmental conditions; thus, it is possible to characterize intraspecific differentiation by analyzing relevant phenotypic traits which, in turn, may be potentially informative of tree adaptability to external factors such as climate. In this study, we focused on two widespread conifers of the Mediterranean basin, black pine and Aleppo pine, that present different evolutionary histories and adaptive divergence [19].

Black pine is a non-serotinous, drought-sensitive species that exits at altitudes ranging from 350 m to 2200 m [20,21]. Different subspecies have been recognized [21,22]: *P. nigra salzmannii* (Dunal) is found in the Iberian Peninsula and Southern France areas; *P. nigra nigra* (Höss) is present in the Apennines, Alps, Balkan Mountains, and Greece; *P. nigra pallasiana* (Lamb.) covers areas in Greece and Turkey; *P. nigra dalmatica* is found in some areas of Croatia; *P. nigra laricio* (Poiret) inhabits the Corsica island; and, finally, *P. nigra calabrica* (Murray) is present in South Italy, although this subspecies is often considered to be *P. nigra* subsp. *laricio*. Previous studies have documented intraspecific variation in miscellaneous traits such as radial growth [23], wood structure [24], total height and tree survival [25], vegetation indices, and reserves [22]. However, genotypic variability of morphological traits has been mainly described for seedling and juvenile stages [26–28]. Aleppo pine is a thermophilic, fire-embracer species with high ecological importance, especially in dry areas due to its drought resistance [29]. Because of its wide distribution range, Aleppo pine is a species with high intraspecific variation (but without subspecies differentiation), which has been described for many functional and life-history traits such as reproduction [30], height growth [2], or photosynthetic indices [15].

Altogether, we expected to find intraspecific differentiation for the analyzed traits in both species as a result of their adaptation to very different ecological niches. However, we hypothesized that this variability, especially regarding crown structure, would be higher in black pine than in Aleppo pine due to the larger phylogeographic divergence of the former. Black pine presents a high morphological variability associated with environmental factors such as snowfall, water availability, and wildfire, which influence crown structure and main trunk growth [31,32]. In this regard, we also hypothesized that the climate at the origin of populations of both pine species could have played an important role in shaping morphological variability of aboveground traits, in agreement with their evolutionary histories and adaptive differentiation. In particular, we expected that black pine populations from a snowy origin had a less dense canopy, while Aleppo pine populations coming from xeric environments showed high aerial growth (e.g., tree height, tree biomass, and crown volume).

2. Materials and Methods

2.1. Study Sites and Field Measurements

This study was carried out in two provenance trials (common gardens) located in Central Spain (Supplementary Table S1). The first trial is located in La Mata de Valsaín, Segovia (degree-minute-second coordinate system: 40°54′42″N, 04°00′50″W). It is composed of 18 populations of adult individuals of *P. nigra*, with subspecies *laricio*, *nigra*, *salzmannii*, *pallasiana*, and *calabrica* (Supplementary Table S1). Seeds were collected in 1995 from 20 to 30 trees of the same populations, spaced at least 100 m apart. They were nursed by following standard container practices [33]. In 1996, 800 one-year-old seedlings were transplanted following a complete randomized block design with 12 replicates, with each experimental unit consisting of a rectangular plot of four seedlings spaced 4.0 × 1.5 m apart. In 2016, the trial was subjected to a systematic thinning by which two out of four trees were logged in each experimental unit to avoid excess competition among trees. A total of 385 trees remained in the trial, and due to trial heterogeneity, we included 345 trees in our analyses (90% of available trees).

The second provenance trial is located in Valdeolmos, Madrid (degree–minute–second coordinate system: 39°49′29″N, 00°34′22″W). It consists of 56 range-wide populations of *P. halepensis* (Aleppo pine; Supplementary Table S2). Seeds were collected by following the same procedure as for *P. nigra*. In 1997, 896 one-year-old seedlings were systematically planted with a distance of 2.5 × 2.5 m, following a complete randomized block design with four replicates. Each experimental unit was composed of four individuals of the same population planted in a linear plot. One block was excluded in this study due to high mortality caused by rabbits during the early plantlet age, and therefore the total number of trees in the trial was 698. Aleppo pine populations were grouped into five

ecotypes according to Patsiou et al. [34], who used a hierarchical cluster analysis to identify ecotypes based on climatic information. These climate-based ecotypes were [34] dry-summer/semiarid/temperate (DST), dry-summer/semiarid/cold (DSC), dry-summer/sub-humid/temperate (DHT), wet-summer/semiarid/temperate (WST), and wet-summer/sub-humid/cool (WHC).

Diameter at breast height (*dbh*) and tree height were measured by using a diameter tape and a Vertex hypsometer, respectively, in February 2022 (Valdeolmos, age 26 years) and in July 2020 (Valsaín, age 25 years), while tree biomass was estimated from published allometric equations at the species level (Table 1).

2.2. Remote Sensing Data Collection

In Valsaín, aerial laser scanning (ALS) records were acquired through an octocopter unmanned aerial vehicle (UAV) equipped with a LiDAR (sensor Velodyne VLP 16 Puck Lite). RGB images were obtained by using a DJI (m300) equipped with a camera having a sensor size of 5472 × 3648 pixels and a focal distance of 8.86 mm. Both flights were performed the same day in July 2020, at an altitude of 40 m and speed of 5 m s^{-1}; the resulting point cloud densities were >500 points/m^2 (LiDAR) and >340 points/m^2 (RGB). In Valdeolmos, ALS data were acquired with an octocopter UAV equipped with LiDAR (sensor Velodyne VLP 32C), whereas an RGB camera with sensor size 6000 × 4000 pixels and focal distance 12 mm was mounted on a DJI (Phantom 4 pro v2) to collect RGB images. Both flights were performed the same day in November 2021, at an altitude of 50 m and speed of 5 m s^{-1}; the resulting point cloud densities were >1000 points/m^2 (LiDAR) and >300 points/m^2 (RGB). Examples of aerial RGB images and LiDAR point clouds are given in Figure 1 for both trials.

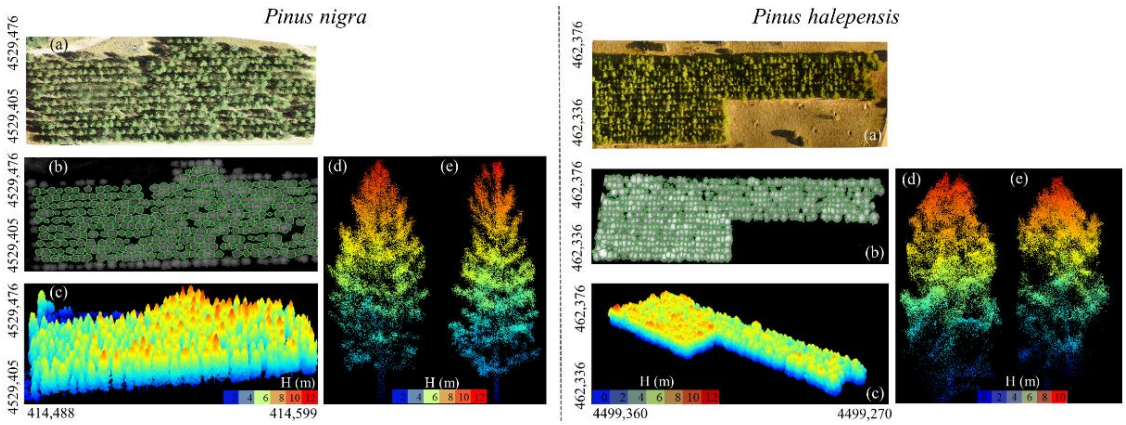


Figure 1. Aerial RGB images and derived information of the two common gardens analyzed in this study (**a**): *Pinus nigra* (left panels) and *Pinus halepensis* (right panels). Example of crown segmentation from the canopy height model of *P. nigra* and *P. halepensis* (**b**). Example of a normalized LiDAR point cloud of *P. nigra* and *P. halepensis* (**c**). Example of extracted tree individual point clouds for *P. nigra* subspecies *nigra* and *laricio* (**d**,**e**), and for Aleppo pine ecotype DHT (**d**) and DSC (**e**).

Table 1. Description of in situ, LiDAR-, and RGB-derived phenotypic traits, along with their function or formula. The traits were obtained for two pine species evaluated in two provenance trials. The first trial was located in Valdeolmos (Madrid province, Spain) and consisted of 56 populations of *Pinus halepensis*. The second trial was located in Valsaín (Segovia province, Spain) and was composed by 18 populations of *Pinus nigra*.

Trait Abbreviation	Trait Description	Function/Formula	Valsaín	Valdeolmos	In Situ	LiDAR-Derived	RGB-Derived
Traits Related to Main Trunk							
h	Total tree height calculated from canopy height model	*Zonal statistic*, QGIS environment	X	X	X	X	X
half h	Half of the total tree height		X	X		X	
dbh	Estimated diameter at breast height	Multilinear model (for UAV-derived *dbh*) for black pine [35] and Aleppo pine [36]	X	X	X	X	X
Traits related to tree biomass							
Ws	Stem biomass	Allometric equation [37]	X	X	X	X	X
Wb2-7	Medium branches biomass	Allometric equation [37]	X	X	X	X	X
Wb2 + n	Thin branches + needles biomass	Allometric equation [37]	X	X	X	X	X
Wr	Root biomass	Allometric equation [37]	X	X	X	X	X
Traits related to crown architecture							
CBH	Height of first living branch	Cubic smooth spline followed by calculation of first and second derivative	X			X	
CL	Total crown length	Total tree height minus *CBH*	X				
CL Skew	Crown height skewness	*skewness* function, R environment	X				
h Skew	Total height skewness	*skewness* function, R environment	X	X		X	
CV_{CL}	Coefficient of variation of crown length point dispersion around the mean	Standard deviation *CL* divided by mean *CL*	X	X		X	

Table 1. *Cont.*

Trait Abbreviation	Trait Description	Function/Formula	Valsaín	Valdeolmos	In Situ	LiDAR-Derived	RGB-Derived
QCD	Crown height quartile coefficient of dispersion	Q1 − Q3/Q1 + Q3	X	X		X	
CA	Crown area calculated from the canopy height model	*Area* function, QGIS	X	X		X	X
h:CA	Ratio between crown height and crown area		X	X		X	X
WCS	Widest crown section	CHM derived tiles with the biggest area				X	
HWCS	Height of widest crown section		X	X		X	
h:HWCS	Total tree height to height of widest crown section ratio		X	X		X	
half h:HWCS	Half tree height to height of widest crown section ratio					X	
RI	Crown height rumple index	*rumple_index* function, R environment	X	X		X	
		Traits related to crown volume					
Q99p	99th percentile of crown's points calculated from the point cloud		X	X		X	
Q75p	75th percentile of crown's points calculated from the point cloud		X	X		X	
Q50p	50th percentile of crown's points calculated from the point cloud		X	X		X	

Table 1. *Cont.*

Trait Abbreviation	Trait Description	Function/Formula	Valsaín	Valdeolmos	In Situ	LiDAR-Derived	RGB-Derived
Q99d	99th percentile of crown's points density calculated from the point cloud		X	X		X	
Q75d	75th percentile of crown's points density calculated from the point cloud		X	X		X	
Q50d	50th percentile of crown's points density calculated from the point cloud		X	X		X	
$Cvol_{025}$	Crown's volume using an alpha value of 0.25 calculated from the point cloud	*alpha shape* function, R environment	X	X		X	
$CH{:}Cvol_{025}$	Ratio between crown height and crown volume		X	X		X	
$3D_{025}{:}2D$	Ratio between $Cvol_{025}$ to crown area		X	X		X	

2.3. Imagery Processing

RGB and LIDAR Preprocessing, Treetop Detection, and Crown Segmentation

The workflow applied to preprocess the LiDAR and RGB point clouds used LAStools [38] and US Forest Service FUSION/LDV 3.42 [39] software. The workflow is summarized in Figure 2. First, we filtered points of noise in the point clouds, using *lasnoise*. Then the ground points were computed with *lasground* and later normalized through the identification of the height above the ground of each point, using *lasheight*. Finally, the points were classified as ground and non-ground (vegetation) through *lasclassify*. Once the data were filtered and classified, we built a digital terrain model (DTM) and a canopy height model (CHM) with a resolution of 10 cm, using the *GridSurfaceCreate* and *CanopyModel* procedures, respectively, of FUSION/LDV. We created slices every 1 m, directly from the LiDAR point clouds, starting from 1 m up to 11 m for Valdeolmos, and from 2 m up to 13 m for Valsaín, and based on this information, we obtained individual CHMs for every slice. These bins were chosen based on the height of the tallest tree and on the thinning strategy applied in Valsaín. For Valdeolmos, we additionally created two slices (one at 0.20 m and another at 0.50 m) because the trial was not pruned, and tree crowns started roughly from the trunk base.

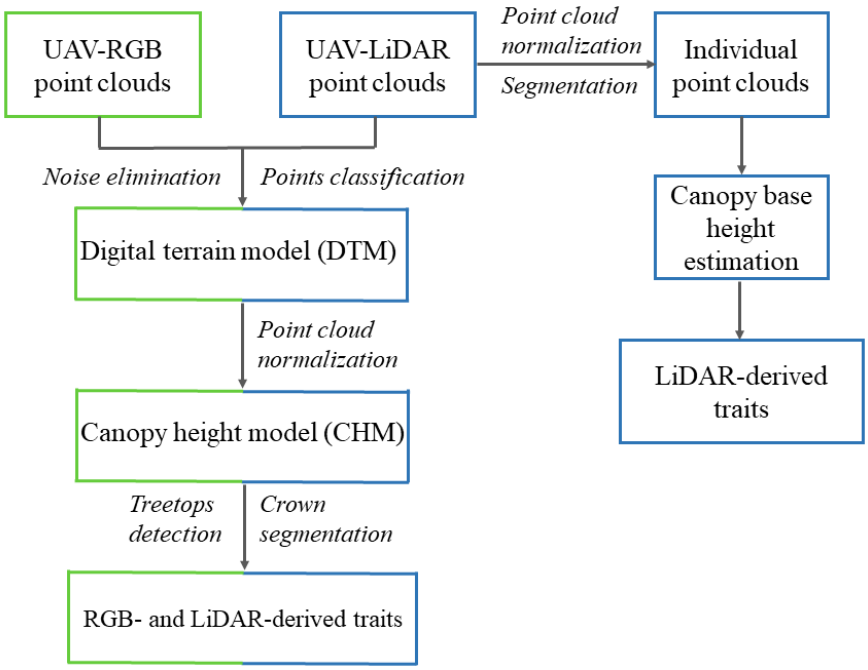


Figure 2. Workflow of RGB and LiDAR point cloud processing. Green lines refer to the RGB-derived point cloud process, and blue lines illustrate the LiDAR-derived point cloud process. The LiDAR-derived traits described in the right part of the workflow are those obtained from the segmentation applied directly to the LiDAR-derived point cloud.

Individual tree detection was performed for each approach independently by using the *vwf* function implemented in the ForestTools R package [40]. This function uses a variable window filter algorithm to detect the local maxima [41] from the canopy height model. We visually evaluated the optimal window size after testing different values. Crowns were automatically segmented, starting from each treetop, using the *mcws* function implemented in ForestTools. We manually corrected the segmented crowns in QGIS in order to eliminate false trees detected by the automatic procedure and, also, to add a segmentation where the algorithm failed to segment a crown. We then proceeded with the segmentation of each CHM slice (only for LiDAR-derived CHM).

Once individual trees were recognized, we calculated the maximum height and crown area for each segmented slice by using first the zonal statistic and then the area function in QGIS.

2.4. LIDAR- and RGB-Derived Traits

We obtained individual tree point clouds for each trial by segmenting the LiDAR-derived normalized point clouds over the respective crown segmented shape file. For Valsaín, we first estimated the crown base height (*CBH*) and, afterward, we obtained several descriptive statistics to characterize the crown architecture of trees, as summarized in Table 1. To estimate *CBH*, we first filtered the point cloud up to 1.3 m, since the trial is pruned and no branches are present below this height value. Then we generated histograms with 0.1 m bins to visualize the vertical distribution of each individual point cloud and applied a cubic smooth spline for which the first and the second derivatives were calculated. Since the inflection points of a smooth spline curve correspond to the zero crossing of their second derivative, we calculated all height values at which the second derivative equaled zero. Then we matched this height value with the closest height at which the number of points within the individual point cloud was minimum [42,43]. In this manner, we were able to identify the *CBH* without mistakenly selecting understory vegetation [43]. We then computed the crown volume by using the alphashape3d R package [44] with an alpha value of 0.25 [45]. Alphashape3d allows for the reconstruct ion of a set of points in a three-dimensional space and produces accurate estimates of crown volume from LiDAR point cloud data [46,47].

We then estimated a rather large set of morphometric characteristics and grouped them into traits related to (i) main trunk, (ii) tree biomass, (iii) crown architecture, or (iv) crown volume (see Table 1 for full details). For Valdeolmos, we did not calculate LiDAR-derived traits relative to *CBH* since this trial had not been pruned and trees could have living or dead branches at ground level. Thus, we just filtered each individual point cloud at 0.20 m to avoid noise originating from small understory shrubs. Afterward, we calculated the same canopy architecture traits as for Valsaín except for *CBH*, crown length (*CL*) and crown skewness (*CL skew*) (Table 1). We also estimated RGB-derived traits, which included total tree height, trunk diameter, tree biomass, crown area, and the ratio between total tree height and crown area (see Table 1).

2.5. Accuracy of Automatic Tree Detection and Validation of UAV-Derived Height and Trunk Diameter

In order to estimate the accuracy of treetop detection, following the local maxima algorithm [38] applied to both LiDAR and RGB canopy height models, we calculated recall (Rc), precision (Pr), and F-score (F) values. R and P represent the completeness and correctness of the detected tree with respect to a reference dataset, respectively, and F is an overall indicator that varies from 0 to 1, with higher values indicating a more accurate segmentation [48]:

$$\mathrm{Rc} = \mathrm{TP}/\mathrm{TP} + \mathrm{FN}, \quad (1)$$

$$\mathrm{Pr} = \mathrm{TP}/\mathrm{TP} + \mathrm{FP}, \quad (2)$$

$$\mathrm{F} = 2 \times (\mathrm{P} \times \mathrm{R}/\mathrm{P} + \mathrm{R}), \quad (3)$$

where TP denotes the number of true positives (trees that are correctly individualized), FP represents the number of false positive (trees that are identified but do not exist), and FN refers to the number of false negative (trees that have not been identified).

Tree height (*h*) and *dbh* measured in situ were used to validate *h* and *dbh* estimates obtained from LiDAR and RGB canopy height models, which were estimated through species-specific allometric equations, using the LiDAR- and RGB-derived tree height and crown area (see Table 1). We used the root mean square error (RMSE), the mean absolute error (MAE), and the coefficient of determination (R^2) statistics for our comparison between the approaches.

2.6. Statistical Analyses

In order to test for population differentiation, traits measured in situ and UAV-derived traits were independently subjected to analysis of variance (ANOVA), with population and replicates as fixed terms for both trials. We also tested for subspecies (black pine) or ecotypic (Aleppo pine) differentiation by partitioning the population term into subspecies (or ecotype) and population nested to subspecies (or ecotype) effects, which were also considered fixed terms. In the latter analysis, two populations of *P. nigra* and four populations of *P. halepensis* were discarded due to their uncertain geographic origin (Supplementary Tables S1 and S2).

In order to reduce the dimensionality of our dataset and evaluate which traits better explained the allometric patterns of subspecies (or ecotypes), we performed a stepwise discriminant analysis for traits that showed significant subspecies (or ecotypic) structure. The significance level corresponding to the F value to be included or excluded in the model was set at $p = 0.15$ [49]. We ran a linear discriminant analysis when the null hypothesis of multivariate normality tested through Mardia's test [50] was not rejected; otherwise, a quadratic discriminant analysis was performed. Moreover, populations' means of traits having a significant population effect were correlated to the climate at the populations' origin. Partial correlations were also applied to the same population means for the purpose of controlling for subspecies (or ecotypic) structure in the dataset. The statistical analyses were performed in SAS/STAT [51].

3. Results

3.1. Accuracy of Tree Detection

The identification of treetops was most accurate when using LiDAR-derived CHM in both provenance trials, showing a recall (R) value of 0.92 and 0.93 for Valsaín and Valdeolmos, respectively. This implied that over 90% of trees were correctly detected at trial level. The overestimation of treetops was quite low (p = 99% for Valsaín; p = 97% for Valdeolmos), and the overall indicator of accuracy, F, was also high (above 95%), indicating accurate treetop identification (Supplementary Table S3). Treetop identification was less accurate when using RGB-derived CHM, although the F was above 91% (Supplementary Table S3).

3.2. Validation with In Situ Measurements

LiDAR-derived *h* and *dbh* estimates were slightly better than RGB-derived estimates for both species, especially for black pine. For this species, LiDAR- and RGB-derived *h* showed an RMSE of 0.36 m and 0.40 m, an MAE of 0.24 m and 0.29 m (Table S4), and an R^2 of 0.92 and 0.90 (Supplementary Figure S1a,b), respectively. The regression between LiDAR- and RGB-derived *h* showed an R^2 of 0.98 (Supplementary Figure S1c). LiDAR- and RGB-derived *dbh* had an RMSE of 1.61 cm and 1.74 cm, an MAE of 1.25 cm and 1.37 cm (Supplementary Table S4), and a an R^2 of 0.67 and 0.65 (Supplementary Figure S2a,b), respectively. The R^2 of the regression between LiDAR- and the RGB-derived *dbh* was 0.95 (Supplementary Figure S2c).

For Aleppo pine, LiDAR- and RGB-derived *h* showed an RMSE of 0.43 m and 0.45 m, an MAE of 0.31 m and 0.34 m (Table S4), and an R^2 of 0.83 and 0.76 (Supplementary Figure S3a,b), respectively. The R^2 of the regression between LiDAR- and RGB-derived *h* was 0.86 (Supplementary Figure S3c). LiDAR- and RGB-derived *dbh* had an RMSE of 1.67 cm and 1.76 cm, an MAE of 1.26 cm (in both cases) (Supplementary Table S4), and an R^2 of 0.73 and 0.69, respectively (Supplementary Figure S4a,b). The regression between LiDAR- and RGB- derived *dbh* showed an R^2 of 0.83 (Supplementary Figure S4c).

3.3. Intraspecific Variability of In Situ Traits and of LiDAR- and RGB-Derived Traits

3.3.1. Black Pine

We detected intraspecific variability for both in situ traits and RGB-derived traits and, also, for most LiDAR-derived traits (Table 2). Significant differences among subspecies

were also found for every trait, showing significant variability among populations, except for two LiDAR-derived traits which exhibited intraspecific variation only at the population level (Table 2).

Table 2. Mixed-effects model analysis of variance for in situ, LiDAR-derived, and RGB-derived phenotypic traits of 18 populations (Pop) of black pine grouped into five subspecies (Subs) grown in a common garden. Only traits with significant population effects are shown in the table. Significant probabilities <0.05 are shown in bold characters.

			In Situ		LiDAR-Derived Traits		RGB-Derived Traits	
Traits	**Effect**	**Num *df***	***F* Value**	***p* > *F***	***F* Value**	***p* > *F***	***F* Value**	***p* > *F***
Traits related to main trunk								
h	Subs	4	8.28	**<0.0001**	8.15	**<0.0001**	7.13	**<0.0001**
	Subs (Pop)	16	1.70	0.0537	1.57	0.0828	1.70	0.0534
half h	Subs	4	/	/	4.16	**0.0032**	/	/
	Subs (Pop)	16	/	/	2.37	**0.0037**	/	/
dbh	Subs	4	6.19	**<0.0001**	4.52	**0.0017**	4.48	**0.0018**
	Subs (Pop)	16	1.49	0.1103	1.21	0.2642	1.31	0.1942
Traits related to tree biomass								
Ws	Subs	4	6.30	**<0.0001**	5.55	**0.0003**	4.96	**0.0008**
	Subs (Pop)	16	1.53	0.0969	1.33	0.1854	1.42	0.1377
Wb2-7	Subs	4	6.16	**0.0001**	4.49	0.0018	4.21	**0.0028**
	Subs (Pop)	16	1.48	**0.0117**	1.18	0.2897	1.27	0.2213
Wb2 + n	Subs	4	6.16	**0.0001**	4.49	**0.0018**	4.21	**0.0028**
	Subs (Pop)	16	1.48	0.1159	1.18	0.2897	1.27	0.2213
Wr	Subs	4	6.05	**0.0002**	4.44	**0.0020**	4.07	**0.0035**
	Subs (Pop)	16	1.45	0.1270	1.	0.3018	1.25	0.2339
Traits related to crown architecture								
CA	Subs	4	/	/	2.70	**0.0328**	2.74	**0.0309**
	Subs (Pop)	16	/	/	0.89	0.5767	0.99	0.4757
h:CA	Subs	4	/	/	2.84	**0.0265**	3.20	**0.0151**
	Subs (Pop)	16	/	/	1.14	0.3281	1.45	0.1253
CL	Subs	4	/	/	9.70	**<0.0001**	/	/
	Subs (Pop)	16	/	/	1.49	0.1120	/	/
WCS	Subs	4	/	/	2.94	**0.0226**	/	/
	Subs (Pop)	16	/	/	0.85	0.6219	/	/
HWCS	Subs	4	/	/	2.51	**0.0447**	/	/
	Subs (Pop)	16	/	/	2.30	**0.0049**	/	/
h:HWCS	Subs	4	/	/	2.19	0.0730	/	/
	Subs (Pop)	16	/	/	0.82	0.6563	/	/
half h:HWCS	Subs	4	/	/	2.53	**0.0433**	/	/
	Subs (Pop)	16	/	/	1.21	0.2694	/	/
h Skew	Subs	4	/	/	5.73	**0.0003**	/	/
	Subs (Pop)	16	/	/	1.89	**0.0257**	/	/
CL Skew	Subs	4	/	/	2.66	**0.0349**	/	/
	Subs (Pop)	16	/	/	1.74	**0.0457**	/	/
QCD	Subs	4	/	/	5.79	**0.0002**	/	/
	Subs (Pop)	16	/	/	1.20	0.2787	/	/
RI	Subs	4	/	/	14.88	**<0.0001**	/	/
	Subs (Pop)	16	/	/	1.29	0.2118	/	/

Table 2. *Cont.*

			In Situ		LiDAR-Derived Traits		RGB-Derived Traits	
Traits	**Effect**	**Num *df***	***F* Value**	***p* > *F***	***F* Value**	***p* > *F***	***F* Value**	***p* > *F***
Traits related to crown volume								
Q99p	Subs	4	/	/	3.83	**0.0055**	/	/
	Subs (Pop)	16	/	/	1.21	0.2670	/	/
Q99d	Subs	4	/	/	2.86	**0.0257**	/	/
	Subs (Pop)	16	/	/	2.61	**0.0013**	/	/
Q75d	Subs	4	/	/	2.92	**0.0234**	/	/
	Subs (Pop)	16	/	/	2.58	**0.0015**	/	/
Q50d	Subs	4	/	/	2.92	**0.0234**	/	/
	Subs (Pop)	16	/	/	2.52	**0.0019**	/	/
CV_{CL}	Subs	4	/	/	8.88	**<0.0001**	/	/
	Subs (Pop)	16	/	/	1.18	0.2926	/	/
$Cvol_{025}$	Subs	4	/	/	4.98	**0.0009**	/	/
	Subs (Pop)	16	/	/	0.96	0.4994	/	/
$H{:}Cvol_{025}$	Subs	4	/	/	2.88	**0.0250**	/	/
	Subs (Pop)	16	/	/	1.11	0.3556	/	/
$3D_{025}{:}2D$	Subs	4	/	/	7.82	**<0.0001**	/	/
	Subs (Pop)	16	/	/	0.95	0.5152	/	/

Three LiDAR-derived traits (coefficient of variation of crown length points (CV_{CL}), crown volume ($Cvol_{025}$), and *h*) discriminated the most among subspecies. The discriminant analysis indicated that the subspecies *calabrica* was associated with a high crown volume, opposite to the subspecies *nigra* (Figure 3a). A low *h*, high $Cvol_{025}$, and high CV_{CL} characterized the subspecies *laricio*, while the subspecies *salzmannii* showed the opposite pattern (Figure 3a). The average squared canonical correlation suggested that ca. 60% of the between-subspecies to within-subspecies variability was explained by the first two discriminant axes, which described 99% of the between-subspecies variation (Figure 3a). The RGB-derived traits that best explained differences among subspecies were *h* and the ratio between height and crown area (*h:CA*), with an average squared canonical correlation of 46% (Table 3). The canonical correlation was a bit higher in the case of in situ traits (68%), with the *h*, *dbh*, and biomass of medium branches as traits that were better at disclosing the differences between subspecies (Table 3).

Table 3. Stepwise discriminant analysis of in situ, LiDAR-derived, and RGB-derived traits of 17 populations of black pine grouped into four subspecies and of 52 populations of Aleppo pine grouped into five ecotypes grown in common gardens in Spain. The only black pine population from subspecies *pallasiana* and four Aleppo pine populations from uncertain geographic origin were not included in the analysis. Partial R^2, significance level, and average squared canonical correlation values are shown for traits entering in the model ($p < 0.15$).

Pinus Nigra						***Pinus Halepensis***					
In Situ Traits						**In Situ Traits**					
Step	**Variable**	**Partial R^2**	***F* Value**	***p* > *F***	**Average Squared Canonical Correlation**	**Step**	**Variable**	**Partial R^2**	***F* Value**	***p* > *F***	**Average Squared Canonical Correlation**
1	*dbh*	0.73	11.46	0.001	0.24	1	*Wb2-7*	0.31	5.20	0.002	0.08
2	*h*	0.85	22.26	<0.001	0.51						
3	*Ws*	0.56	4.64	0.025	0.68						

Table 3. *Cont.*

Pinus Nigra						*Pinus Halepensis*					
In Situ Traits						**In Situ Traits**					
Step	**Variable**	**Partial R^2**	***F* Value**	***p* > *F***	**Average Squared Canonical Correlation**	**Step**	**Variable**	**Partial R^2**	***F* Value**	***p* > *F***	**Average Squared Canonical Correlation**
UAV–LiDAR-derived traits						UAV–LiDAR-derived traits					
1	CV_{CL}	0.87	28.83	<0.001	0.29	1	*Q75d*	0.29	4.76	0.003	0.07
2	$Cvol_{025}$	0.77	13.27	<0.001	0.54	2	CV_{CL}	0.31	5.24	0.002	0.15
3	*h*	0.70	8.61	0.003	0.60						
UAV–RGB-derived traits						UAV–RGB-derived traits					
1	*h*	0.71	10.54	0.001	0.24	1	*Wb2-7*	0.22	3.29	0.019	0.06
2	*h:CA*	0.69	8.89	0.002	0.46	2	*dbh*	0.14	1.91	0.126	0.09
						3	*h*	0.19	2.54	0.053	0.13

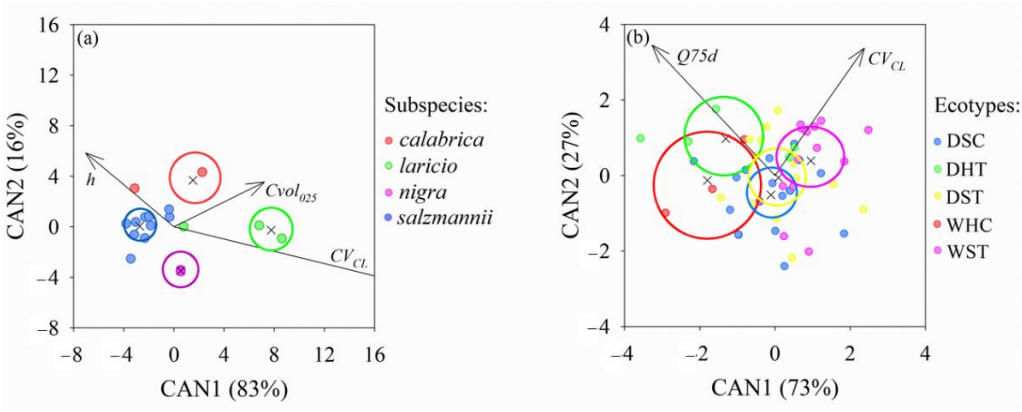


Figure 3. Discriminant analysis plots showing the centroids (black crosses) and their 95% confidence ellipses for the first two canonical variables (CAN1 and CAN2) for four subspecies of *P. nigra* (**a**) and five ecotypes of *P. halepensis* (**b**) and their explanatory variables, using LiDAR-derived traits. $Cvol_{025}$ = crown volume calculated with alpha equal to 0.25; *h* = total tree height; CV_{CL} = coefficient of variation of crown length point dispersion; *Q75d* = 75th percentile of crown's point density calculated from the point cloud.

3.3.2. Aleppo Pine

Tree biomass (stem biomass (*Ws*), medium branches biomass (*Wb2-7*), thin branches and needles biomass (*Wb2* + *n*) and root biomass (*Wr*)) and main trunk growth traits (*h* and *dbh*) showed significant population effects in the case of in situ traits, and also for both remote-sensing-derived approaches (Table 4). Additionally, LiDAR-derived traits showed intraspecific variability also for main trunk traits (specifically, *half h*), crown architecture traits (height of the widest crown section (*HWCS*), height skewness (*h skew*), CV_{CL}, and quartile coefficient dispersion of crown length points (*QCD*)), and crown volume traits (density of points at 99th, 75th, and 50th quartiles (*Q99d*, *Q75d*, and *Q50d*, respectively) and ratio of crown volume to crown area ($Cvol_{025}$*:CA*)). All traits mentioned above showed a significant ecotypic structure, except for three LiDAR-derived traits (Table 4).

The discriminant analysis summarized the ecotypic structure for the species by means of two LiDAR-derived traits: CV_{CL} and *Q75d* (Table 3; Figure 3b). The analysis indicated that ecotype DHT had a denser canopy, as opposed to ecotypes DST and DSC, while ecotype WST showed a high CV_{CL} values (Figure 3b). However, the average squared canonical correlation was low, thereby indicating a relatively low discrimination, with the first two discriminant axes explaining only 15% of the between- to within-ecotype

variability (Table 3). Three RGB-derived traits (*h*, *dbh*, and *Wb2-7*) discriminated the most among ecotypes; however, only 13% of the between- to within-ecotype variability was explained by the first two discriminant axes (Table 3). Regarding in situ traits, only the biomass of medium branches was identified in the stepwise discriminant analysis (Table 3).

Table 4. Mixed-effects model analysis of variance for in situ, LiDAR-derived, and RGB-derived phenotypic traits of 52 populations (Pop) of Aleppo pine grouped into five ecotypes grown in a common garden. Only traits with significant population effects are shown in the table. Significant probabilities <0.05 are shown in bold characters.

			In Situ		LiDAR-Derived Traits		RGB-Derived Traits	
Trait	**Effect**	**Num *df***	***F* Value**	***p* > *F***	***F* Value**	***p* > *F***	***F* Value**	***p* > *F***
Traits related to main trunk								
h	Ecotype	4	2.96	**0.0196**	4.22	**0.0023**	5.54	**0.0002**
	Pop (Ecotype)	47	2.41	**<0.0001**	2.71	**<0.0001**	2.65	**<0.0001**
half h	Ecotype	4	/	/	4.22	**0.0023**	/	/
	Pop (Ecotype)	47	/	/	2.71	**<0.0001**	/	/
dbh	Ecotype	4	6.28	**<0.0001**	2.79	**0.0261**	2.49	**0.0426**
	Pop (Ecotype)	47	1.54	**0.0152**	1.81	**0.0012**	1.60	**0.0088**
Traits related to tree biomass								
Ws	Ecotype	4	8.52	**<0.0001**	5.09	**0.0005**	5.11	**0.0005**
	Pop (Ecotype)	47	1.46	**0.0285**	1.87	**0.0007**	1.73	**0.0026**
Wb2-7	Ecotype	4	8.76	**<0.0001**	5.32	**0.0003**	4.93	**0.0007**
	Pop (Ecotype)	47	1.38	0.0539	1.67	**0.0048**	1.68	**0.0045**
Wb2 + n	Ecotype	4	8.52	**<0.0001**	5.06	**0.0005**	5.06	**0.0005**
	Pop (Ecotype)	47	1.44	**0.0334**	1.79	**0.0015**	1.69	**0.0038**
Wr	Ecotype	4	8.10	**<0.0001**	3.72	**0.0055**	3.00	**0.0182**
	Pop (Ecotype)	47	1.44	**0.0334**	1.75	**0.0021**	1.47	**0.0265**
Traits related to crown architecture								
HWC	Ecotype	4	/	/	3.68	**0.0058**	/	/
	Pop (Ecotype)	47	/	/	1.85	**0.0009**	/	/
h Skew	Ecotype	4	/	/	1.98	0.0967	/	/
	Pop (Ecotype)	47	/	/	1.59	**0.0101**	/	/
CV_{CL}	Ecotype	4	/	/	4.30	**0.0020**	/	/
	Pop (Ecotype)	47	/	/	1.27	0.1126	/	/
QCD	Ecotype	4	/	/	1.81	0.1251	/	/
	Pop (Ecotype)	47	/	/	1.50	**0.0206**	/	/
Traits related to crown volume								
Q99d	Ecotype	4	/	/	7.38	**<0.0001**	/	/
	Pop (Ecotype)	47	/	/	1.33	0.0762	/	/
Q75d	Ecotype	4	/	/	7.27	**<0.0001**	/	/
	Pop (Ecotype)	47	/	/	1.33	0.0757	/	/
Q50d	Ecotype	4	/	/	5.54	**0.0002**	/	/
	Pop (Ecotype)	47	/	/	1.31	0.0903	/	/
3D025:2D	Ecotype	4	/	/	1.92	0.1068	/	/
	Pop (Ecotype)	47	/	/	2.35	**<0.0001**	/	/

3.4. Relationships between In Situ or UAV Traits and Climate at Populations' Origin

3.4.1. Black Pine

The LiDAR-derived traits showing a larger number of significant correlations with climate at the origin of populations were those related to the main trunk (*h*), crown architecture (ratio between tree height and widest crown section (*h:HWCS*), *h skew*, CV_{CL}, and *QCD*), and crown volume (*Q99d*, *Q75d*, and *Q55d*) (Figure 4a). The latter traits related to crown density also showed negative correlations with altitude. Traits related to crown architecture showed a positive correlation with longitude, mean annual precipitation (MAP), and precipitation of the wettest quarter and winter precipitation (PwtQ and Pw, respectively) and a negative correlation with temperature annual range (TAR) (Figure 4a). TAR was the climate variable with highest number of significant relationships with the entire set of traits analyzed. This variable showed negative associations with traits descriptive of tree height, regardless of the approach used for its estimation, and canopy architecture (Figure 4a).

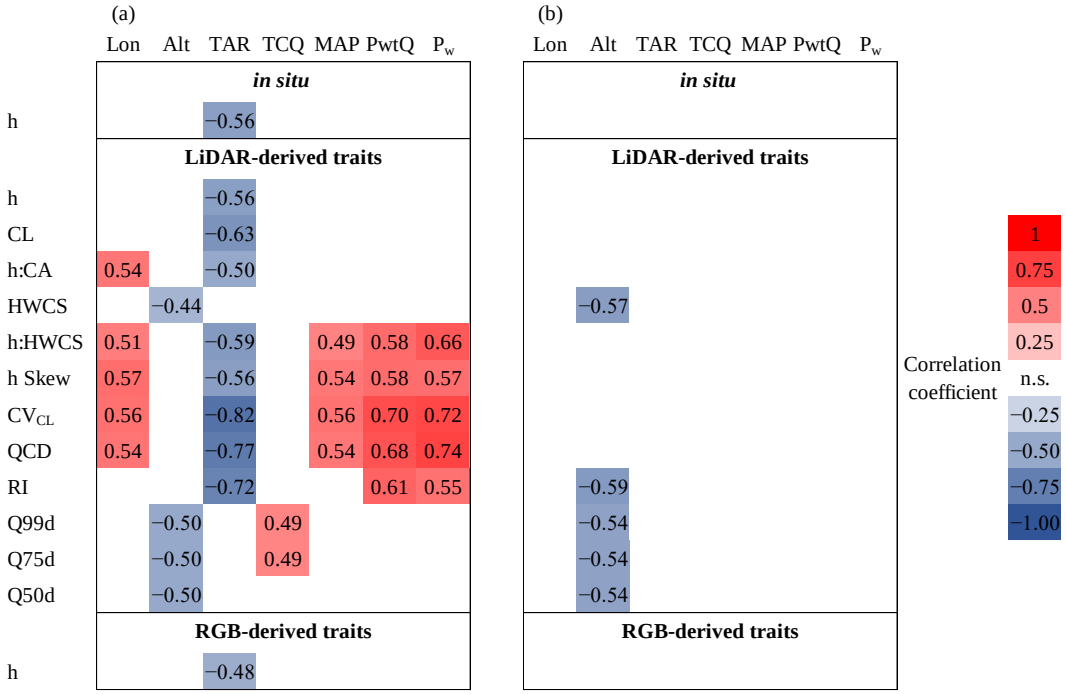


Figure 4. Simple correlation (a) and partial correlation coefficients (b) between population means of in situ, RGB-derived, or LiDAR-derived traits and climate factors at populations' origin for 16 populations of *Pinus nigra* tested in a common garden located in Valsaín (Spain). Only significant correlations ($p < 0.05$) with their respective correlation coefficients are shown.

After accounting for the subspecies structure, TAR was no longer the most influential climate variable, suggesting that all previously significant correlations were driven by large differences among subspecies (Figure 4b). This pattern was also common to any other significant correlation described above, except for three traits related to crown volume and two traits related to crown architecture, which were negatively related to altitude (Figure 4b).

3.4.2. Aleppo Pine

In situ measures of trunk diameter and estimates of tree biomass were positively correlated with longitude, MAP, and PwtQ and negatively correlated with altitude and TAR (Figure 5). Regarding RGB-derived traits, only those related to tree biomass showed significant correlations with climate. In particular, *Wb2-7* and *Wb + n* showed the same correlation pattern as for in situ measures, while the remaining RGB-derived biomass traits showed significant relationships with TAR (negative) and with MAP and PwtQ (positive)

(Figure 5). The same pattern was found for LiDAR-derived *Wb2 + n*, while *Wb2-7* was also negatively correlated to altitude and positively correlated to longitude. Additionally, *Ws* was positively correlated with PwtQ and MAP, and *Wr* had a positive correlation with MAP only. Crown volume traits such as *Q99d*, *Q75d*, and *Q50d* showed positive correlations with longitude, and *Q75d* had also a negative correlation with altitude. Similarly, a negative correlation with altitude was observed for *HWCS*, which also had a negative correlation with TAR. Finally, CV_{CL} was positively correlated with the temperature of the coldest quarter (TCQ) (Figure 5).

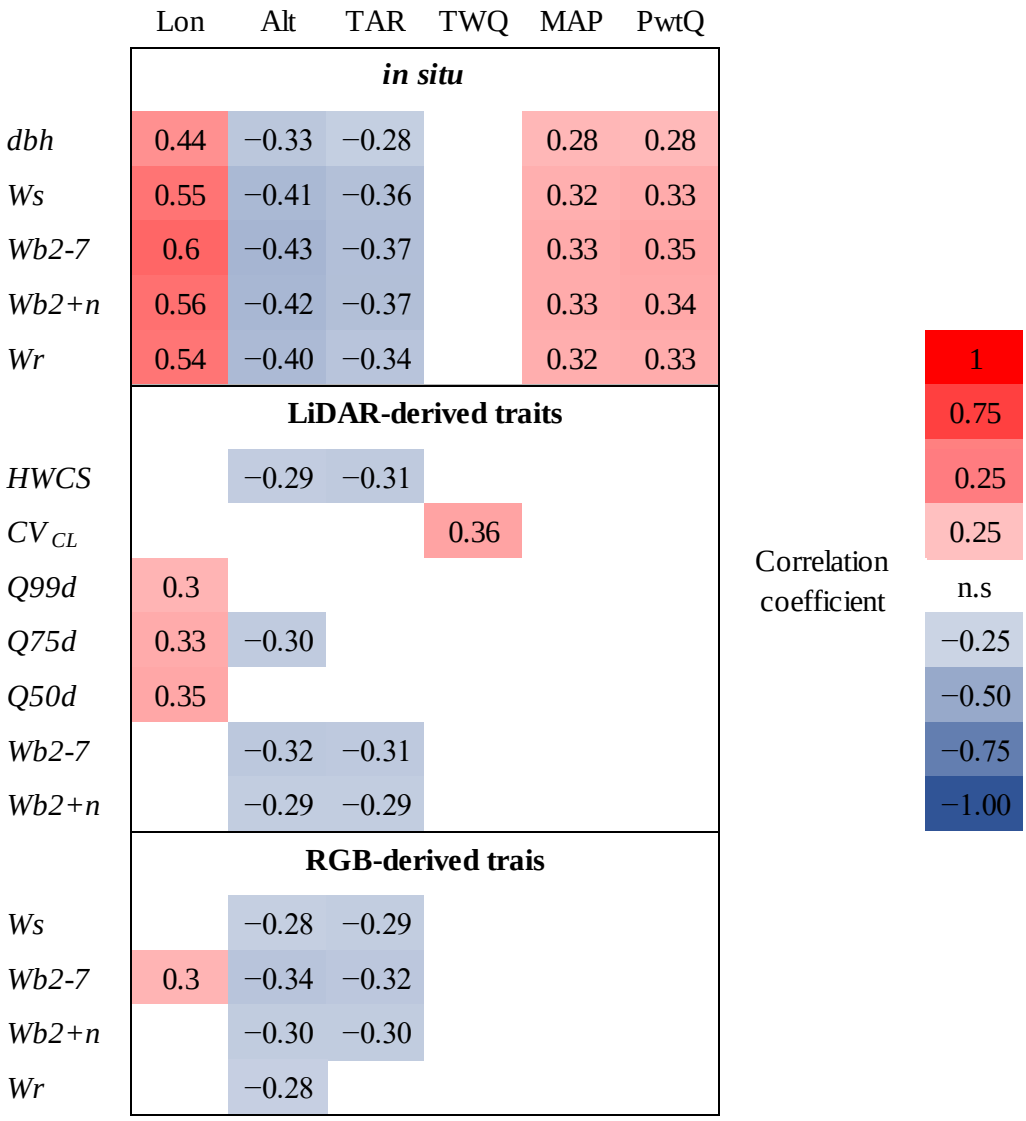


Figure 5. Simple correlation coefficients between population means of in situ, RGB-derived, or LiDAR-derived traits and climate factors at populations' origin for 48 populations of Aleppo pine tested in a common garden located in Valdeolmos (Spain). Only significant correlations ($p < 0.05$) with their respective correlation coefficients are shown.

Partial correlations accounting for differences among ecotypes did not show any significant relationship between the analyzed traits and the climate at origin of populations, suggesting a lack of finer-scale ecogeographic patterns beyond the ecotypic structure of the species (results not shown).

4. Discussion

This study applied high-throughput UAV-based phenotyping techniques for the assessment of genetic differentiation in regard to the morphological traits of two widespread Mediterranean pines (black pine and Aleppo pine). In particular, the effectiveness of LiDAR and RGB imagery was investigated to characterize tree phenotypes and their variability at the population and meta-population (subspecies and ecotypes) level. Thus, we demonstrated the potential of these indirect approaches to disclose tree architectural differences potentially related to intraspecific adaptive divergence in pine species.

4.1. Tree Segmentation Accuracy and Field Validation

Our study showed that individual tree detection and segmentation obtained from UAV–LiDAR had a slightly higher overall accuracy than that obtained through UAV–RGB for both pine species. However, it also indicated that trees correctly identified and segmented by using UAV–RGB were over 90%, which is still an excellent outcome compared to other studies involving alternative forest tree species growing in natural conditions such as *Pinus sylvestris* L., *Picea abies* (L.) *H. Karts.*, and *Quercus rubra* L., among others [52], and in line with similar studies performed in common gardens [7,16].

The validation of LiDAR- and RGB-derived tree height and *dbh* against in situ measurements indicated that UAV–LiDAR estimated tree height and *dbh* better than UAV–RGB in both species, and especially for black pine, which showed a lower estimated error and a higher R^2. The fact that treetops and tree height were estimated with more accuracy and less error in black pine compared to Aleppo pine might be attributable to the thinning and pruning treatments applied in Valsaín, which produced a sparser canopy cover. As a result, more ground points could be easily classified within the point clouds, generating a more accurate DTM [13,53] and, subsequently, a more accurate CHM from which tree height could be estimated with better accuracy. In addition, we speculate that morphological differences between these species, especially related to canopy architecture (denser in Aleppo pine) and total tree height (higher in black pine), could have also influenced accuracy, as described in previous studies for mixed temperate forests [35]. We would like to emphasize that, even though RGB imagery is less expensive than aerial LiDAR, both methods showed high accuracy in the identification of individual trees and, also, in the estimation of morphological traits commonly used in forest studies, such as *dbh* and total tree height.

4.2. Intraspecific Differentiation in Black Pine and Associations with Climate at Origin

This study emphasizes the great intraspecific variability of growth traits and crown structure in European black pine. In particular, our results showed that populations belonging to *P. nigra* ssp. *nigra* presented the lowest aerial growth, regardless of methodology (in situ, LiDAR-derived, or RGB-derived). Conversely, populations from South Italy, belonging to the subspecies *calabrica*, showed the opposite pattern. These results are in line with previous studies that described *P. nigra* ssp. *nigra* as a slow-growing [22], but highly frost-tolerant species [27]. Thus, traits related to crown structure could also be related to the large cold hardiness of this subspecies, especially crown density. Indeed, a slender, shorter, and sparser canopy may shield the tree from snow canopy damage, as previously described for other pine species [31,54].

Furthermore, according to our findings, intraspecific variability in crown complexity and shape indicates genetic differentiation in growth habit that may be related to particular responses to environmental stresses such as drought, snowfall, and fire. Particularly, populations originating from mesic environments (i.e., Corsica), which belong to the subspecies *laricio*, showed a higher crown volume and a more expanded crown. These populations have been described as less conservative, fast growing [22], and frost sensitive [27] than populations from xeric areas (i.e., Iberian Peninsula), belonging to the subspecies *salzmannii*, which showed the opposite pattern. The Iberian subspecies occupies areas in the southernmost distribution range of black pine, where drought and snowfall are the main limiting

factors for growth; however, some growth differences seem to exist between southern and northern populations within this region [55,56]. Southernmost populations occupy a higher altitude, so they are subject to intense summer drought but also to heavy snowfalls in winter. These populations may have undergone more intense selection wherein snow is a key selective factor that influences crown structure [57]. This was hinted at by our results, in which the partial correlation analysis suggested that altitude was the only environmental variable showing an eco-geographic pattern beyond the subspecies structure of black pine.

Fire intensity and frequency can also play an important role for this fire-tolerant species [58], and the fact that populations from the xeric environment showed a smaller and more homogeneous crown and a lower height in which the widest crown is found might be the result of selective factors that prioritize reserve accumulation and traits potentially related to surface fire-resistance that can facilitate survival under moderate-intensity surface fires [32] at the expense of aboveground growth.

4.3. Intraspecific Differentiation in Aleppo Pine and Associations with Climate at Origin

Significant variation was detected in Aleppo pine at the population and ecotype level for many in situ, as well as LiDAR- and RGB-derived, traits. As hypothesized, however, ecotypic differentiation was by far less structured and somehow blurry compared to the strong subspecies structure exhibited by *P. nigra*.

Populations belonging to ecotypes WST and DSC (native to the Balearic Islands, Italy, and the Central–South Iberian Peninsula) showed lower primary growth and crown volume. This is in clear contrast to populations from France, Northern Spain, and Greece, belonging to ecotypes WHC and DHT, which presented the opposite pattern. The latter ecotypes, originating from mesic environments, are characterized by higher phenotypic plasticity and generally grow faster than their counterparts from xeric areas [34,59]. The observed pattern can be the result of an adaptive syndrome in which populations from the east Mediterranean basin and from mesic origins invest more in aboveground growth compared to other plant compartments related to reproduction [30] or roots [60] and also to water-use efficiency [61], among others. This can also be interpreted as a genetically based shade-avoidance strategy adopted by ecotypes from more favorable environments and therefore subject to higher competition, since a more expanded crown might enhance light capture and carbon gain [62]. These features may indeed reduce the negative effect of competition [63]. On the other hand, some morphological traits related to tree biomass, *dbh*, and crown architecture showed a negative relationship with altitude and continentality (annual range temperature), thereby highlighting the thermophilic characteristic of this species [64]. In addition, as fire-embracer species [58], Aleppo pine populations (and ecotypes) from xeric environments could assign more resources to reproduction, in particular to the production of serotine cones as a post-fire regeneration strategy, at the expense of other functional traits related, e.g., primary growth [32]. The limited height and lower height at which the widest crown is found may indeed enhance tree flammability, favoring surface fire to become crown fire [65].

5. Conclusions

This study demonstrated the adequacy of two remote sensing approaches (UAV–LiDAR and UAV–RGB) in assessing the genetic variability of morphometric traits in adult trees of pine species at the intraspecific level. UAV–LiDAR accuracy was slightly better for the identification of individual trees and for the estimation of *dbh* and total tree height. However, the accuracy of UAV–RGB was still very good, and, depending on the objective and available resources of the study, it might be appropriate to trade some accuracy for affordability. We conclude that genetic differentiation in tree structural differences potentially driven by environmental conditions at origin of populations of pine species can be effectively disclosed by using UAV-based high-throughput phenotyping approaches. Indeed, these methods also overcome the complex and time-consuming traditional measures of adult trees under field conditions.

Supplementary Materials: The following supporting information can be downloaded at. https://www.mdpi.com/article/10.3390/rs14225904/s1. Figure S1: Linear regressions between in situ measured *h* and LiDAR- or RGB-derived *h* of black pine. Figure S2: Linear regressions between in situ measured *dbh* and LiDAR- or RGB-derived *dbh* of black pine. Figure S3: Linear regressions between in situ measured *h* and LiDAR- or RGB-derived *h* of Aleppo pine. Figure S4: Linear regressions between in situ measured *dbh* and LiDAR- or RGB-derived *dbh* of Aleppo pine. Table S1: Name, code, subspecies, geographic origin, and environmental conditions of 18 populations of European black pine. Table S2: Name, code, subspecies, geographic origin, and environmental conditions of 18 populations of Aleppo pine. Table S3: Treetops accuracy detection of the local maxima algorithm applied to LiDAR and RGB canopy-height models. Table S4: Validation of *h* and *dbh* derived from LiDAR and RGB canopy-height models against *h* and *dbh* measured in situ.

Author Contributions: Conceptualization, J.V.; methodology, E.L., F.R.-P. and F.S.; formal analysis, E.L., F.R.-P. and J.V.; investigation, E.L., F.R.-P., M.R.C., J.C. and J.V.; writing—original draft preparation, E.L.; writing—review and editing, F.R.-P., F.S., M.R.C., J.C., V.R.d.D. and J.V.; supervision, V.R.d.D. and J.V.; funding acquisition, V.R.d.D. and J.V. All authors have read and agreed to the published version of the manuscript.

Funding: This work was partly supported by the Spanish Government, grant numbers RTI2018-094691-B-C31 and RTI2018-094691-B-C33 (MCIU/AEI/FEDER, EU). E. Lombardi was supported by a AGAUR FI-2021 pre-doctoral fellowship (with the support from the Secretariat for Universities and Research of the Ministry of Business and Knowledge of the Government of Catalonia and the European Social Fund).

Data Availability Statement: The data supporting the results of this study are available at the CORA open repository (https://dataverse.csuc.cat/, accessed on 12 October 2022).

Acknowledgments: We are grateful to E. Chacón-Moreno and A. Morera for fieldwork and technical assistance.

Conflicts of Interest: The authors declare no conflict of interest.

References

1. Poorter, L.; Lianes, E.; Moreno-de las Heras, M.; Zavala, M.A. Architecture of Iberian canopy tree species in relation to wood density, shade tolerance and climate. *Plant Ecol.* **2012**, *213*, 707–722. [CrossRef]
2. Voltas, J.; Shestakova, T.A.; Patsiou, T.; di Matteo, G.; Klein, T. Ecotypic variation and stability in growth performance of the thermophilic conifer *Pinus halepensis* across the mediterranean basin. *For. Ecol. Manag.* **2018**, *424*, 205–215. [CrossRef]
3. Karna, Y.K.; Penman, T.D.; Aponte, C. Remote sensing assessing legacy effects of wildfires on the crown structure of fire-SAR and LIDAR Fusion: Experiments and applications. *Remote Sens.* **2019**, *11*, 2433. [CrossRef]
4. Grote, R.; Gessler, A.; Hommel, R.; Poschenrieder, W.; Priesack, E. Importance of tree height and social position for drought-related stress on tree growth and mortality. *Trees—Struct. Funct.* **2016**, *30*, 1467–1482. [CrossRef]
5. Ordóñez, J.L.; Retana, J.; Espelta, J.M. Effects of tree size, crown damage, and tree location on post-fire survival and cone production of *Pinus nigra* trees. *For. Ecol. Manag.* **2005**, *206*, 109–117. [CrossRef]
6. Lombardi, E.; Shestakova, T.A.; Santini, F.; Resco de Dios, V.; Voltas, J. Harnessing tree-ring phenotypes to disentangle gene by environment interactions and their climate dependencies in a circum-Mediterranean pine. *Ann. Bot.* **2022**, *130*, 509–523. [CrossRef]
7. Liao, L.; Cao, L.; Xie, Y.; Luo, J.; Wang, G. Phenotypic traits extraction and genetic characteristics assessment of eucalyptus trials based on UAV-borne LiDAR and RGB images. *Remote Sens.* **2022**, *14*, 765. [CrossRef]
8. Leite, R.V.; Silva, C.A.; Mohan, M.; Cardil, A.; de Almeida, D.R.A.; e Carvalho, S.d.P.C.; Jaafar, W.S.W.M.; Hernández, J.G.; Weiskittel, A.; Hudak, A.T.; et al. Individual tree attribute estimation and uniformity assessment in fast-growing *Eucalyptus* Spp. forest plantations using Lidar and linear mixed-effects models. *Remote Sens.* **2020**, *12*, 3599. [CrossRef]
9. Ganz, S.; Käber, Y.; Adler, P. Measuring tree height with remote sensing-a comparison of photogrammetric and LiDAR data with different field measurements. *Forests* **2019**, *10*, 694. [CrossRef]
10. Camarretta, N.; Harrison, P.A.; Lucieer, A.; Potts, B.M.; Davidson, N.; Hunt, M. From drones to phenotype: Using UAV-LiDAR to detect species and provenance variation in tree productivity and structure. *Remote Sens.* **2020**, *12*, 3184. [CrossRef]
11. Liu, Q.; Fu, L.; Chen, Q.; Wang, G.; Luo, P.; Sharma, R.P.; He, P.; Li, M.; Wang, M.; Duan, G. Analysis of the spatial differences in canopy height models from UAV LiDAR and photogrammetry. *Remote Sens.* **2020**, *12*, 2884. [CrossRef]
12. Moe, K.T.; Owari, T.; Furuya, N.; Hiroshima, T.; Morimoto, J. Application of UAV photogrammetry with Lidar data to facilitate the estimation of tree locations and Dbh values for high-value timber species in Northern Japanese mixed-wood forests. *Remote Sens.* **2020**, *12*, 2865. [CrossRef]

13. Mielcarek, M.; Kamińska, A.; Stereńczak, K. Digital Aerial Photogrammetry (DAP) and Airborne Laser Scanning (ALS) as sources of information about tree height: Comparisons of the accuracy of remote sensing methods for tree height estimation. *Remote Sens.* **2020**, *12*, 1808. [CrossRef]
14. Goodbody, T.R.H.; Coops, N.C.; White, J.C. Digital aerial photogrammetry for updating area-based forest inventories: A review of opportunities, challenges, and future directions. *Curr. For. Rep.* **2019**, *5*, 55–75. [CrossRef]
15. Solvin, T.M.; Puliti, S.; Steffenrem, A. Use of UAV photogrammetric data in forest genetic trials: Measuring tree height, growth, and phenology in Norway spruce (*Picea abies* L. Karst.). *Scand. J. For. Res.* **2020**, *35*, 322–333. [CrossRef]
16. Santini, F.; Kefauver, S.C.; Resco de Dios, V.; Araus, J.L.; Voltas, J. Using Unmanned Aerial Vehicle-based multispectral, RGB and thermal imagery for phenotyping of forest genetic trials: A case study in *Pinus halepensis*. *Ann. Appl. Biol.* **2019**, *174*, 262–276. [CrossRef]
17. du Toit, F.; Coops, N.C.; Tompalski, P.; Goodbody, T.R.H.; El-Kassaby, Y.A.; Stoehr, M.; Turner, D.; Lucieer, A. Characterizing variations in growth characteristics between Douglas-fir with different genetic gain levels using airborne laser scanning. *Trees—Struct. Funct.* **2020**, *34*, 649–664. [CrossRef]
18. Colaço, A.F.; Trevisan, R.G.; Molin, J.P.; Rosell-Polo, J.R.; Escolà, A. A method to obtain orange crop geometry information using a mobile terrestrial laser scanner and 3D modeling. *Remote Sens.* **2017**, *9*, 763. [CrossRef]
19. Tapias, R.; Climent, J.; Pardos, J.A.; Gil, L. Life histories of Mediterranean pines. *Plant Ecol.* **2004**, *171*, 53–68. [CrossRef]
20. Enescu, C.M.; de Rigo, D.; Caudullo, G.; Mauri, A.; Houston Durrant, T. Pinus nigra in Europe: Distribution, habitat, usage and threats. In *European Atlas of Forest Tree Species*; San- Miguel-Ayanz, J., de Rigo, D., Caudullo, G., Houston Durrant, T., Mauri, A., Eds.; EU Office: Luxembourg, 2016; pp. 126–127.
21. Isajev, V..; Fady, B.; Semerci, H..; Andonovski, V. *EUFORGEN Technical Guidelines for Genetic Conservation and Use for European Black Pine (Pinus nigra)*; International Plant Genetic Resources Institute: Rome, Italy, 2003; 6p.
22. Santini, F.; Serrano, L.; Kefauver, S.C.; Abdullah-Al, M.; Aguilera, M.; Sin, E.; Voltas, J. Morpho-physiological variability of *Pinus nigra* populations reveals climate-driven local adaptation but weak water use differentiation. *Environ. Exp. Bot.* **2019**, *166*, 103828. [CrossRef]
23. Fkiri, S.; Guibal, F.; Fady, B.; El Khorchani, A.; Khaldi, A.; Khouja, M.L.; Nasr, Z. Tree-rings to climate relationships in nineteen provenances of four black pines sub-species (*Pinus nigra Arn.*) growing in a common garden from northwest Tunisia. *Dendrochronologia* **2018**, *50*, 44–51. [CrossRef]
24. Esteban, L.G.; Martín, J.A.; de Palacios, P.; Fernández, F.G. Influence of region of provenance and climate factors on wood anatomical traits of *Pinus nigra Arn*. subsp. *salzmannii. Eur. J. For. Res.* **2012**, *131*, 633–645. [CrossRef]
25. Varelides, C.; Brofas, G.; Varelides, Y. Provenance variation in *Pinus nigra* at three sites in Northern Greece. *Ann. For. Sci.* **2001**, *58*, 893–900. [CrossRef]
26. Bachofen, C.; Perret-Gentil, A.; Wohlgemuth, T.; Vollenweider, P.; Moser, B. Phenotypic plasticity versus ecotypic differentiation under recurrent summer drought in two drought-tolerant pine species. *J. Ecol.* **2021**, *109*, 3861–3876. [CrossRef]
27. Kreyling, J.; Wiesenberg, G.L.B.; Thiel, D.; Wohlfart, C.; Huber, G.; Walter, J.; Jentsch, A.; Konnert, M.; Beierkuhnlein, C. Cold hardiness of *Pinus nigra Arnold* as influenced by geographic origin, warming, and extreme summer drought. *Environ. Exp. Bot.* **2012**, *78*, 99–108. [CrossRef]
28. Topacoglu, O. Genetic diversity among populations in black pine (*Pinus Nigra Arnold*. Subsp. *Pallasiana (Lamb.) Holmboe) seed stands in Turkey. Bulg. J. Agric. Sci.* **2013**, *19*, 1459–1464.
29. Chambel, M.R.; Climent, J.; Pichot, C.; Ducci, F. Mediterranean pines (*Pinus halepensis Mill.* and *brutia Ten.*). In *Forest Tree Breeding in Europe. Managing Forest Ecosystems*; Pâques, L., Ed.; Springer: Dordrecht, The Netherlands, 2013; Volume 25, pp. 229–265.
30. Climent, J.; Prada, M.A.; Calama, R.; Chambel, M.R.; De Ron, D.S.; Alía, R. To grow or to seed: Ecotypic variation in reproductive allocation and cone production by young female Aleppo pine (*Pinus halepensis*, *pinaceae*). *Am. J. Bot.* **2008**, *95*, 833–842. [CrossRef] [PubMed]
31. Stevens, J.T.; Kling, M.M.; Schwilk, D.W.; Varner, J.M.; Kane, J.M. Biogeography of fire regimes in Western U.S. conifer forests: A trait-based approach. *Glob. Ecol. Biogeogr.* **2020**, *29*, 944–955. [CrossRef]
32. Aubrey, D.P.; Coleman, M.D.; Coyle, D.R. Ice damage in loblolly pine: Understanding the factors that influence susceptibility. *For. Sci.* **2007**, *53*, 580–589.
33. Landis, T.D. Containers type and functions. In *The Container Tree Nursery Manual, Landis*; Tinus, R.W., McDonald, S.E., Barnett, J.P., Eds.; USDA Forest Service: Washington, DC, USA, 1990; Volume 2, pp. 1–39.
34. Patsiou, T.S.; Shestakova, T.A.; Klein, T.; di Matteo, G.; Sbay, H.; Chambel, M.R.; Zas, R.; Voltas, J. Intraspecific responses to climate reveal nonintuitive warming impacts on a widespread thermophilic conifer. *New Phytol.* **2020**, *228*, 525–540. [CrossRef] [PubMed]
35. Balenović, I.; Jazbec, A.; Marjanović, H.; Paladinić, E.; Vuletić, D. Modeling tree characteristics of individual black pine (*Pinus Nigra Arn.*) trees for use in remote sensing-based inventory. *Forests* **2015**, *6*, 492–509. [CrossRef]
36. Aguilar, F.J.; Nemmaoui, A.; Aguilar, M.A.; Jiménez-Lao, R. Aleppo pine allometric modeling through integrating UAV Image-Based point clouds and ground-based data. *ISPRS Ann. Photogramm. Remote Sens. Spat. Inf. Sci* **2022**, *V-3-2022*, 353–360. [CrossRef]
37. Ruiz-Peinado, R.; Rio, M.; Montero, G. New models for estimating the carbon sink capacity of Spanish softwood species. *For. Syst.* **2011**, *20*, 176–188. [CrossRef]

38. Isenburg, M. LAStools-Efficient LiDAR Processing Software, Version 141017, Academic 2017. Available online: http://rapidlasso.com (accessed on 2 May 2022).
39. McGaughey, R.J. *FUSION/LDV: Software for LIDAR Data Analysis and Visualization, Version 3.50*; US Department of Agriculture, Forest Serivce, Pacific Northwest Research Station, University of Washington: Seattle, WA, USA, 2015.
40. Plowright, A.; Plowright, M.A. R Package 'ForestTools'. CRAN. 2018. Available online: https://github.com/andrew-plowright/ForestTools (accessed on 5 June 2022).
41. Popescu, S.C.; Wynne, R.H. Seeing the trees in the forest: Using LIDAR and multispectral data fusion with local filtering and variable window size for estimating tree height. Photogramm. *Eng. Remote Sens.* **2004**, *70*, 589–604. [CrossRef]
42. Arkin, J.; Coops, N.C.; Daniels, L.D.; Plowright, A. Estimation of vertical fuel layers in tree crowns using high density lidar data. *Remote Sens.* **2021**, *13*, 4598. [CrossRef]
43. Luo, L.; Zhai, Q.; Su, Y.; Ma, Q.; Kelly, M.; Guo, Q. Simple method for direct crown base height estimation of individual conifer trees using airborne LiDAR data. *Opt. Express* **2018**, *26*, A562. [CrossRef]
44. Lafarge, T.; Pateiro-Lopez, B. Alphashape3d: Implementation of the 3D Alpha-Shape for the Reconstruction of 3D Sets from a Point Cloud. 2017. Available online: https://cran.r-project.org/package=alphashape3d (accessed on 3 July 2022).
45. Ahongshangbam, J.; Khokthong, W.; Ellsäßer, F.; Hendrayanto, H.; Hölscher, D.; Röll, A. Drone-based photogrammetry-derived crown metrics for predicting tree and oil palm water use. *Ecohydrology* **2019**, *12*, e2115. [CrossRef]
46. Korhonen, L.; Vauhkonen, J.; Virolainen, A.; Hovi, A.; Korpela, I. Estimation of tree crown volume from airborne Lidar data using computational geometry. *Int. J. Remote Sens.* **2013**, *34*, 7236–7248. [CrossRef]
47. Yan, Z.; Liu, R.; Cheng, L.; Zhou, X.; Ruan, X.; Xiao, Y. A Concave hull methodology for calculating the crown volume of individual trees based on vehicle-borne LiDAR data. *Remote Sens.* **2019**, *11*, 623. [CrossRef]
48. Neuville, R.; Bates, J.S.; Jonard, F. Estimating forest structure from UAV-Mounted LiDAR point cloud using machine learning. *Remote Sens.* **2021**, *13*, 35. [CrossRef]
49. Dillon, W.R.; Goldstein, M. *Multivariate Analysis: Methods and Applications*; Wiley: Hoboken, NJ, USA, 1984; pp. 360–393.
50. Mardia, K.V. Measures of multivariate skewness and kurtosis with applications. In *Biometrika*; Oxford University Press: Oxford, UK, 1970; Volume 57, pp. 519–530.
51. Littell, R.C.; Henry, P.R.; Ammerman, C.B. Statistical analysis of repeated measures data using SAS procedures. *J. Anim. Sci.* **1998**, *76*, 1216–1231. [CrossRef]
52. Vauhkonen, J.; Ene, L.; Gupta, S.; Heinzel, J.; Holmgren, J.; Pitkänen, J.; Solberg, S.; Wang, Y.; Weinacker, H.; Hauglin, K.M.; et al. Comparative testing of single-tree detection algorithms under different types of forest. *Forestry* **2012**, *85*, 27–40. [CrossRef]
53. Reutebuch, S.E.; Mc Gaughey, R.J.; Andersen, H.E. Accuracy of an IFSAR-Derived digital terrain model under a conifer forest canopy. *Can. J. Remote Sens.* **2005**, *31*, 283–288. [CrossRef]
54. Fish, H.; Lieffers, V.J.; Silins, U.; Hall, R.J. Crown shyness in lodgepole pine stands of varying stand height, density, and site index in the upper foothills of Alberta. *Can. J. For. Res.* **2006**, *36*, 2104–2111. [CrossRef]
55. Navarro-Cerrillo, R.M.; Sánchez-Salguero, R.; Manzanedo, R.D.; Camarero, J.J.; Fernández-Cancio, Á. Site and age condition the growth responses to climate and drought of relict *Pinus nigra* Subsp. *salzmannii* populations in southern Spain. *Tree-Ring Res.* **2014**, *70*, 145–155. [CrossRef]
56. Amodei, T.; Guibal, F.; Fady, B. Relationships between climate and radial growth in black pine (*Pinus nigra arnold* ssp. *salzmannii* (dunal) franco) from the south of France. *Ann. For. Sci.* **2013**, *70*, 41–47. [CrossRef]
57. Climent Maldonado, J.M.; Sierra de grado, R. El derecho a crecer torcido: ¿es adaptativa la rectitud del tronco? In Proceedings of the VII Congreso Forestal Español, Plasencia, Spain, 26–30 June 2017.
58. Resco de Dios, V.; Arteaga, C.; Hedo, J.; Gil-Pelegrín, E.; Voltas, J. A Trade-off between embolism resistance and bark thickness in conifers: Are drought and fire adaptations antagonistic? *Plant Ecol. Divers.* **2018**, *11*, 253–258. [CrossRef]
59. Ramírez-Valiente, J.A.; del Santos del Blanco, L.; Alía, R.; Robledo-Arnuncio, J.J.; Climent, J. Adaptation of Mediterranean forest species to climate: Lessons from common garden experiments. *J. Ecol.* **2022**, *110*, 1022–1042. [CrossRef]
60. Lombardi, E.; Ferrio, J.P.; Rodríguez-Robles, U.; Resco de Dios, V.; Voltas, J. Ground-Penetrating Radar as phenotyping tool for characterizing intraspecific variability in root traits of a widespread conifer. *Plant Soil* **2021**, *468*, 319–336. [CrossRef]
61. Voltas, J.; Lucabaugh, D.; Chambel, M.R.; Ferrio, J.P. Intraspecific variation in the use of water sources by the circum-Mediterranean conifer *Pinus halepensis*. *New Phytol.* **2015**, *208*, 1031–1041. [CrossRef]
62. Duursma, R.A.; Mäkelä, A. Summary models for light interception and light-use efficiency of non-homogeneous canopies. *Tree Physiol.* **2007**, *27*, 859–870. [CrossRef]
63. Brisson, J. Neighborhood competition and crown asymmetry in *Acer saccharum*. *Can. J. For. Res.* **2001**, *31*, 2151–2159. [CrossRef]
64. Vennetier, M.; Ripert, C.; Rathgeber, C. Autecology and growth of Aleppo pine (*Pinus halepensis Mill.*): A comprehensive study in France. *For. Ecol. Manag.* **2018**, *413*, 32–47. [CrossRef]
65. Ne'eman, G.; Goubitz, S.; Nathan, R. Reproductive traits of *Pinus halepensis* in the light of fire—A critical review. *Plant Ecol.* **2004**, *171*, 69–79. [CrossRef]